Morphology and Viscoelastic Properties of Melt-Spun HDPE/Hydrotalcite Nanocomposite Fibers

Luca Fambri,[1,2] Izabela Dabrowska,[1,2] Giuseppe Ferrara,[3] Alessandro Pegoretti[1,2]
[1]*Department of Industrial Engineering, University of Trento, Via Sommarive 9, 38123 Trento, Italy*

[2]*National Interuniversity Consortium for Science and Technology of Materials (INSTM), Via G. Giusti 9, 50121 Firenze, Italy*

[3]*LyondellBasell Industries-Centro Ricerche "Giulio Natta," P.le Donegani 12, 44100 Ferrara, Italy*

Viscoelastic properties of nanocomposite fibers of high density polyethylene (HDPE) and organically modified hydrotalcite were studied. Neat and nanofilled HDPE fibers (with nanofiller content between 0.5 and 3 wt%) were produced by melt spinning and hot-drawing at different draw ratios up to 20. Effect of temperature on storage modulus, loss modulus, and creep compliance were compared. Rising nanofiller content and/or drawing ratio accounted for an increase in storage modulus in the glassy (i.e., below the γ transition at $-100^{\circ}C$) as well as in the rubbery state of non-crystalline regions. The α relaxation temperature read-off for the maximum of the loss modulus peak ranged from 20 to 60°C being dependent on frequency, filler content and draw ratio. Sumita model was successfully applied to evaluate the effective volume fraction of the dispersed phase; maximum fraction of immobilized matrix was observed for the composite with 1 wt% of nanofiller. Creep behavior was evaluated by fitting experimental data with the Burgers model. The addition of a small amount of well-dispersed hydrotalcite (0.5–1 wt%) had a beneficial effect on the creep resistance of drawn fibers at room temperature as well as at 70°C. TEM analysis evidenced a good dispersion of 0.5% nanofiller in as-spun fibers and improved interfacial adhesion after drawing. The best mechanical properties were observed for the composition with 1 wt% of hydrotalcite, due to combined effects of nanofiller reinforcement and stiffening produced by hot drawing. POLYM. COMPOS., 37:288–298, 2016. © 2014 Society of Plastics Engineers

INTRODUCTION

Owing to favorable combination of good tensile properties, flexibility, low cost, and chemical resistance, polyethylene has been used in a wide range of industrial applications, such as piping systems, bags, bottles, ropes, fibers, etc. [1]. Commercial polyolefine fibers are produced not only from homopolymers, such as high density polyethylene (HDPE) and isotactic polypropylene (iPP), but also from copolymers, for example ethylene-propylene, ethylene-octene or even ethylene-propylene-butene, and multifilaments where each filament contains a PP core and a PE sheath. PP/PE bicomponent fibers are widely used for non-woven fabrics production [2, 3]. Broad range of applications requires the control and the modifications of thermo-mechanical properties and creep behavior. One of the recent research topics is the introduction of different types of nanofillers into the polymer matrix, for instance the layered double hydroxides (LDH) frequently referred to as hydrotalcites. Synthetic anionic mineral clays similar to silica clays [4] are composed of positively charged metal hydroxide sheets with intercalated anions and water molecules in the interlayer region. Moreover, LDH modification is usually performed to enlarge the interlayer distance of the pristine clay, to increase the hydrophobic nature and to reduce the interaction between platelets, and hence to facilitate the dispersion in polyolefins. Organically modified hydrotalcite can easily be melt-dispersed and exfoliated forming a true nanocomposite with improved properties, e.g., a higher stiffness and thermal degradation stability [4–8]. For specific applications, as rope and high performance fibers, melt spinning of high molecular weight polymer and subsequent drawing are convenient to produce high stiffness and high strength polyethylene [9].

On the other hand, relatively few studies have been published on fiber spinning and drawing of polyolefin nanocomposites. La Mantia et al. [10] observed the increase in the elastic modulus and tensile strength of LLDPE/nanoclay composite fibers at high draw ratios, which has been attributed to the alignment of polymer chains and clay particles along the strain direction, which allows for a strong interfacial load transfer.

Correspondence to: L. Fambri; e-mail: luca.fambri@unitn.it
DOI 10.1002/pc.23180
Published online in Wiley Online Library (wileyonlinelibrary.com).

Moreover, Zhang et al. [11] confirmed that nanofilled fibers show a higher degree of crystallinity because the nanofiller acts as a nucleating agent for a larger number of smaller crystals during the hot-drawing process, which is beneficial for the mechanical properties of UHMWPE fiber. In the case of PP/LDH fibers, Guo et al. [12] observed a good exfoliation and uniform dispersion conferring superior thermal stability on the nanocomposite fibers. Simultaneously, a slight improvement of mechanical properties was found due to the presence of relatively high amount of compatibilizer which, however, somewhat weakens the reinforcing effect of LDH.

Solid state mechanical properties of polymers are strongly affected by molecular motions related to the glass transition temperature and to the secondary transitions (in the glassy state) routinely observed by means of the dynamic mechanical experiments [13]. The transitions of polyethylene labeled as the α-, β-, and γ-transitions occur in the intervals about 30/100°C, −30/10°C, and −150/−120°C, respectively [14, 15]. The α transition is generally ascribed to the amorphous parts of semicrystalline polymers, however the authors dealing with PE have violated previously established molecular interpretation of the α (glass transition), β (secondary transition), γ (low-temperature transition) transitions. The α transition/relaxation in PE is attributed to the main chain movements along the c-axis of the crystals which involves shear and reorientation movements along the c-axis of the crystal lamella [13–16]. The α loss peak is sometimes split into two α and α' peaks, which are both ascribed to the crystalline phase [13, 16]. The β relaxation is related to the motions of short disordered chain, as in LDPE and LLDPE [17]. Similar results were observed by Dechter et al. [18] in NMR-measurements, where a quite high mobility of the chains in the amorphous regions was detected. In linear HDPE, the β relaxation is usually very weak (or is not observed at all) due to high degree of crystallinity and almost complete? absence of branching [19]. The crystal lamellae hinder molecular mobility in the minority amorphous phase underlying the β transition up to the temperatures of the α relaxation taking place in the crystalline regions [16]. Although both α and β transitions were investigated by several research groups, the effect of the crystal morphology (lamella thickness, crystal structure, crystallinity content) on these relaxations is not yet completely understood. Finally, the γ relaxation is identified with the motion of three to four methylene groups (crankshaft motions) and is commonly viewed as the glass transition temperature of polyethylene [13].

In recent literature, melt compounding of HDPE with hydrotalcite (LDH) nanoparticles was reported to improve thermal stability and mechanical properties [20–22]. Melt spinning of HDPE/LDH nanocomposites has been recently described by Dabrowska et al. [5] and Kutlu et al. [23]. Using low melt flow (0.9 dg min^{-1}) and high melt flow (34 dg min^{-1}) polymers with nanofiller up to 3% by wt, they reported tenacity of the produced as-spun fibers in the range of 0.4–0.6 cN/dtex and 0.2–0.3 cN/dtex, respectively. Following these findings, high molecular weight HDPE was considered the most promising matrix for the high strength (high performance) fibers. Subsequently, Fambri et al. obtained tenacity of drawn nanocomposite fibers in the range of 3–10 cN/dtex, corresponding to about 0.3–1.0 GPa [6]. Studying the viscoelastic behavior, D'Amato et al. specified the role of filler in the stiffening of drawn HDPE fibers containing 2% of fumed nanosilica; a higher storage modulus master curve and a lower creep compliance were observed [24].

The objective of this work was to investigate the effect of the LDH content on the viscoelastic behavior of drawn PE/LDH nanocomposite fibers. For this purpose, dynamical mechanical thermal analysis (DMTA) and creep measurements were used. The stiffness and damping characteristic of the prepared nanocomposite fibers are related to (i) the morphology (TEM analysis) and to (ii) the variation of the α transition with the molecular orientation induced by drawing. Storage modulus is used to visualize the stiffening effect as a function of processing, whereas loss modulus data are compared to evaluate the LDH dispersion with the aid of the Sumita model. Creep compliance results are also presented and various composite fibers are compared by using the Burgers model.

EXPERIMENTAL SECTION

Materials and Sample Preparation

Material. High density polyethylene HDPE Eltex® A4009 (melt flow rate 0.85 dg min^{-1} at 190°C/2.16 kg; density 0.96 g cm^{-3}) in the form of fine powder was supplied by BP Solvay (Brussels, Belgium).

Masterbatch pellets of synthetic hydrotalcite organically modified with fatty acid, Perkalite F100 (AkzoNobel; density 1.35–1.40 g cm^{-3}) was provided by Clariant Masterbatches S.p.A.-Italy at 12% by wt. of nanofiller, and 12% by wt. of polyethylene grafted with maleic anhydride (HDPE-g-MA) as compatibilizer. Before the processing, masterbatch was dried at 90°C in a vacuum oven for 24 h. Nanocomposites were designated as hydrotalcite abbreviation (LDH) and the filler percentage by wt. As an example, LDH-2 indicates a nanocomposite fiber containing 2 wt% of hydrotalcite.

Fiber Spinning and Drawing. Fibers were produced in a double step process, i.e. extrusion and hot-drawing (the composition is given in Table 1). After compounding the mixture of HDPE, compatibilizer and nanofiller by Thermo Haake PTW16 intermeshing co-rotating twin screw extruder ($D = 16$ mm, $L/D = 25$), monofilaments of about 500 μm diameter were spun from a rod die diameter 1.65 mm. The temperature profile was gradually increased from the hopper (130°C) to the rod die (220°C). The spun fibers were cooled in cold water and were wrapped around a cylinder at 8 m min^{-1}.

Drawn fibers were obtained in a hot-plate drawing apparatus 140 cm length (SSM-Giudici srl, Galbiate, LC, Italy) at temperature of 125°C, a constant feeding rate of 1.2 m min^{-1} and various collecting rate. Draw ratio (DR) is defined according to *Eq. 1*, as the ratio between the cross section of the initial (S_i) and final fiber (S_f)

$$DR = \frac{S_i}{S_f} = \left(\frac{D_i}{D_f}\right)^2 \quad (1)$$

where D_i and D_f are the initial and final diameter of the fiber.

The diameter of the fiber was measured by using an optical microscope (Table 1) with an image processing software (ImageJ®). Fibers at three different draw ratio DR = 5, 10, and 20, were selected, and compared to the as-spun fiber (DR = 1). Other details of production have been reported in literature [6].

Experimental Techniques

Ultramicrotomed cross section of the as-spun nanocomposite fibers were used for the TEM analysis in order to get information on nanofiller distribution, by using a FEI Tecnai 10 Transmission Electron Microscope (TEM), operated at cryogenic temperatures (lower than −70°C).

Dynamic mechanical thermal analysis (DMTA) was carried out with the DMA Q800 testing dynamometer (TA Instruments). As-spun and drawn fibers were tested in tensile mode by using a fiber clamp (gauge length of 10 mm; pre-stress of 0.01 N; sinusoidal strain with a frequency of 1 Hz and amplitude of 64 μm) from −125 to 125°C with a heating rate of 3°C min^{-1}. Storage modulus and loss modulus were measured as functions of temperature [25].

Creep response of drawn and undrawn fibers was studied at 30°C and at 70°C by using a dynamic mechanical analyzer DMA Q800 (TA Instruments): gauge length of 10 mm; constant stress (σ_0) of 3 MPa ; creeping time of 3600 s. The chosen creep stress corresponded to about 10% of the yield stress of undrawn fiber [5].

RESULTS AND DISCUSSION

TEM

Selected LDH nanocomposite fibers were previously studied by using SEM and XRD analysis [5, 6]. The compositions containing 1 and 2 wt% of LDH exhibited fine filler dispersion with various clusters of about 0.3 and 1.5 μm in as-spun fibers, which evidenced intercalation and partial exfoliation in drawn fibers with draw ratio of 10 and 15. On the other hand, clusters of about 2 μm in LDH-3 as-spun fibers were found; according to XRD analysis no intercalation was achieved even at high draw ratios.

TABLE 1. Designation, composition (wt%) and diameter of HDPE nanocomposite fibers as functions of the draw ratio (DR).

	HDPE	LDH-0.5	LDH-1	LDH-2	LDH-3
Composition					
HDPE (%)	100	99	98	96	94
LDH (%)	0	0.5	1	2	3
HDPE-*g*-MA (%)	0	0.5	1	2	3
Diameter of fiber (micron)					
DR = 5	210 ± 3	210 ± 1	211 ± 3	210 ± 3	209 ± 1
DR = 10	155 ± 2	155 ± 3	153 ± 2	155 ± 1	154 ± 3
DR = 20	109 ± 2	110 ± 2	110 ± 1	110 ± 1	111 ± 2

TEM images of ultramicrotomed cross section of nanofilled LDH-0.5 HDPE fibers at different draw ratios are presented in Fig. 1, in order to illustrate the morphology and dispersion of hydrotalcite in nanocomposite fibers. Figure 1a reveals that as-spun and undrawn fibers (DR = 1) are characterized by the presence of uniformly dispersed hydrotalcite particles in the form of aggregates with size of about 0.5–2 μm. In the same time, the tendency to a partial intercalation is documented in micrographs at higher magnifications (Fig. 1b and c). Low level of LDH intercalation in the polymer matrix after melt spinning is probably the reason of very similar tensile properties of the as-spun unfilled and nanofilled fibers [6]. Similar observations were also reported in the case of HDPE/fumed nanosilica fibers [24].

It is worth noting that at drawing ratios DR = 5 and DR = 20 (Fig. 1d–h), a higher level of LDH intercalation can be observed, which documents the effect of the drawing process on the microstructure. For DR = 5, particle sizes in the range from 200 nm up to 500 nm (Fig. 1d) were detected, thus evidencing partial exfoliation (Fig. 1e). For DR = 20, even better dispersion of the LDH particles was obtained (Fig. 1f), and low particle size of about 100 nm could be observed (Fig. 1g and h). We can conclude that the drawing process induces the rupture of hydrotalcite aggregates and controls the intercalation and/or partial exfoliation of LDH in the HDPE matrix, which accounts for improvement of the mechanical properties of nanofilled fibers.

Dynamic Mechanical Thermal Analysis

Fibers with different draw ratios were studied to obtain deeper information on mechanical properties and molecular mobility. Storage modulus (E') and loss modulus (E'') of neat HDPE and nanocomposites in the range −125/+125°C are presented in Fig. 2a–d for undrawn fibers, and fibers drawn 5, 10, and 20 times.

Two transitions, namely γ and α at about −120 and 45°C were observed, similarly to the case of HDPE/LDH plates [5]. Figure 2a shows the progressive decrease in storage modulus with temperature in correspondence to these two loss modulus peaks, while there is absolutely no evidence of the β transition at about

 DOI 10.1002/pc

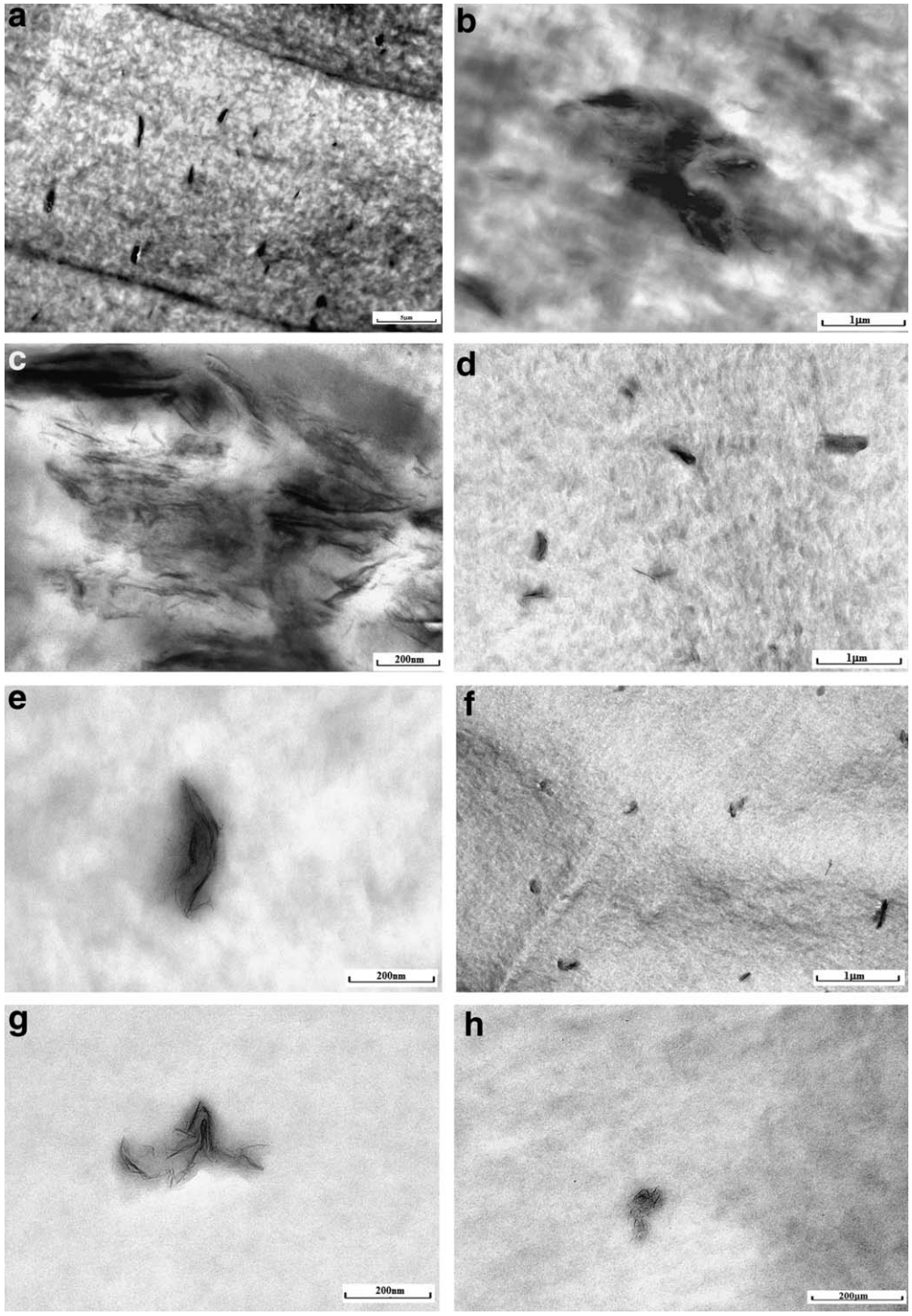

FIG. 1. a–c. TEM images of ultra-microtomed cross-section of undrawn nanocomposite fibers at various magnifications. d,e. TEM images of ultra-microtomed cross-section of drawn nanocomposite fiber (DR = 5) at various magnifications. f–h. TEM images of ultra-microtomed cross-section of drawn nanocomposite fibers (DR = 20) at various magnifications.

−50°C. However, the temperatures of the α loss peak in the range 38–47°C for as-spun fibers (Table 2) are rather different from those reported in the literature survey, for instance at 52–59°C for HDPE plates of identical LDH composition [6].

Storage Modulus. Storage modulus of LDH-2 and LDH-3 as-spun fibers (DR = 1) was found slightly higher than that of HDPE at low temperatures (from −100°C up to −30°C). On the other hand, at temperatures higher than 0°C, all of the compositions exhibited almost the

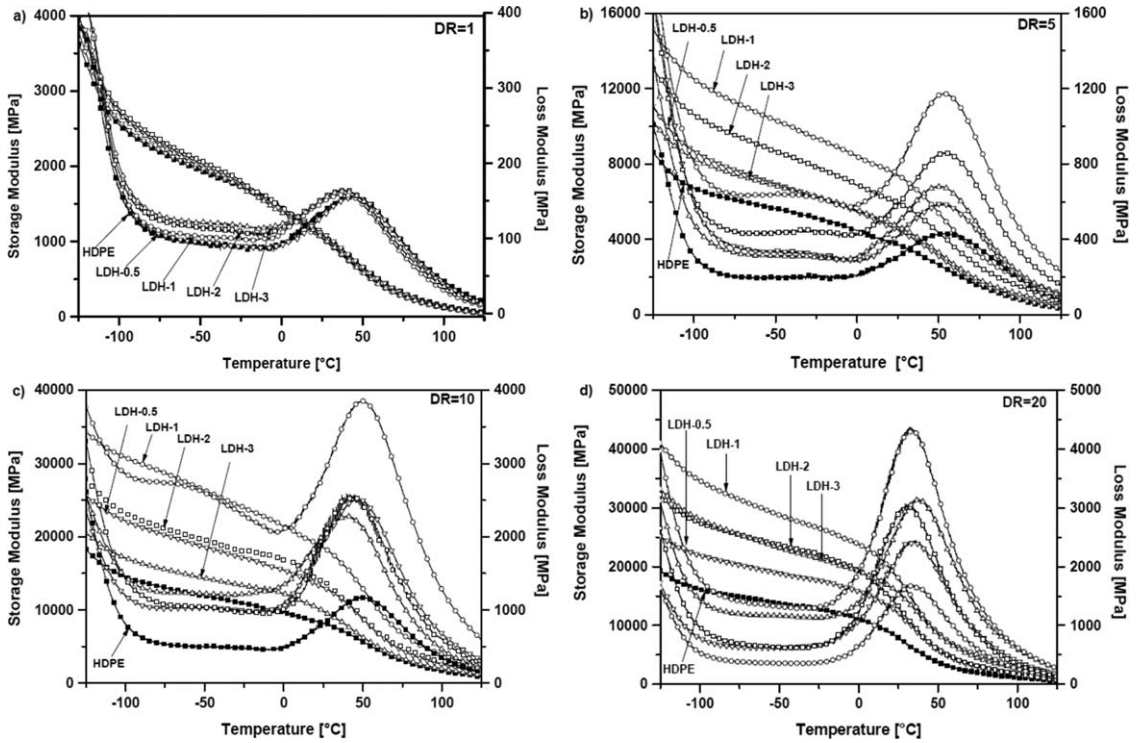

FIG. 2. Storage modulus and loss modulus of neat HDPE (■) and nanocomposite HDPE fibers with different amount of hydrotalcite (▽−0.5%, ○-1%, □-2% and Δ −3%) at different draw ratio (a) DR = 1, (b) DR = 5, (c) DR = 10, and (d) DR = 20.

same storage modulus, for instance about 1.1 GPa at 30°C and about 0.4 GPa at 70°C (Fig. 2a).

Incorporated hydrotalcite increases storage modulus (E') of composite drawn fibers, which is shown in Fig. 2b–d for DR = 5, DR = 10, and DR = 20, respectively. As expected, the higher the drawing ratio, the higher the storage modulus in all ranges of tested temperatures and compositions, which is a result of the molecular orientation induced by stretching. However, the effect of the nanofiller content is not linear, in fact a relative maximum of storage modulus of drawn fibers was found at the composition LDH-1, as evidenced in Table 2 and in Fig. 3. At LDH contents higher than 1 wt%, the decrease in storage modulus could be attributed to the uneven dispersion and the tendency of the nanofiller to form agglomerates [26]. In fact, XRD analysis of the composition with 3 wt% of LDH reported in previous paper confirmed that nanofiller was not exfoliated [6].

The storage modulus variation can be summarized as follows

$$\text{HDPE} < \text{LDH-0.5},\ \text{LDH-3} \leq \text{LDH-2} < \text{LDH-1}$$

Similar tendency was observed for polyolefine/LDH composites [23, 26, 27]. Kontou and Niaounakis explain this behavior by the co-existence of (i) a free bulk matrix and (ii) an interphase formed by polyethylene molecules

TABLE 2. Temperature of the α loss peak (Tα), selected storage modulus, and intensity of the transition (S-factor) of the nanocomposite fibers with different LDH content and/or DRs.

	DR = 1			DR = 5			DR = 10			DR = 20		
Fiber	Tα (°C)	$E'_{-30°C}/E'_{90°C}$ (MPa)	S	Tα (°C)	$E'_{-30°C}/E'_{90°C}$ (MPa)	S	Tα (°C)	$E'_{-30°C}/E'_{90°C}$ (MPa)	S	Tα (°C)	$E'_{-30°C}/E'_{90°C}$ (MPa)	S
HDPE	45.0	1769/200	7.8	53.4	5239/990	4.3	50.0	11129/2071	4.4	34.0	13231/1549	7.5
LDH-0.5	47.0	1784/202	7.8	51.8	6400/1058	5.0	46.4	17519/3136	4.6	33.0	18042/2176	7.3
LDH-1	38.7	1846/173	9.7	54.6	9621/2290	3.2	50.0	24517/4657	4.3	33.0	27246/3850	6.1
LDH-2	38.3	1882/175	9.7	55.0	8046/1811	3.4	46.0	18279/3440	4.3	32.0	22435/2178	9.3
LDH-3	38.3	1793/164	9.9	50.0	6403/1263	4.1	39.0	13563/2375	4.7	36.5	21808/3222	5.7

Heating rate: 3°C min^{-1}; frequency: 1 Hz.

 DOI 10.1002/pc

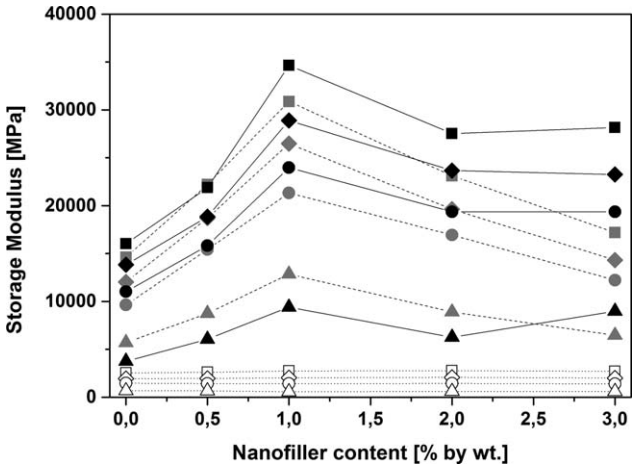

FIG. 3. Variation of the storage modulus of HDPE fibers with nanofiller content. Temperatures: ■ −100°C,◆ −50°C, ▼ 0°C, ▲ 25°C and ● 50°C. Draw ratios: (a) open symbol—DR = 1, (b) grey symbol—DR = 10, (c) black symbol—DR = 20.

adsorbed on the filler's surface [28], which depends on a good dispersion and/or on the aggregate formation. The initial increase in the nanofiller amount enlarges the interfacial area and, consequently, the volume fraction of interphase, where limited molecular motions account for an increase in storage modulus. However, at a higher nanofiller content, the filler aggregates reduce the interfacial adhesion between matrix and filler, which may account for a lower storage modulus.

The effect of the filler on HDPE and drawn fibers was also studied by using the intensity of the α transition (S), calculated according to the *Eq. 2*

$$S=(E'_{-30}-E'_{-90})/E'_{90} \quad (2)$$

where E'_{-30} and E'_{-90} are storage moduli read off below and above the α transition temperature [29]. Intensity S of the transition is proportional to the fraction and molecular mobility of the phase involved in the transition (for instance the amorphous phase of partially crystalline polymers giving rise to the glass transition). S-factor was found to increase in composites where the filler induced a higher stiffening of the glassy phase than of the rubbery phase [30]. Table 2 shows *S* values between 7.8 and 9.9 for as-spun fiber; in the case of drawn fibers with DR = 5–10, the S factor decreased in the range 3.2–5.0, probably due to reduced mobility of the polymer chains after drawing process. During spinning a high orientation of macromolecular chains and a consecutive enhancement of the crystallinity content were reported [6]. For draw ratio DR = 20, the *S* factor of both HDPE and LDH nanocomposite fibers was found in the range 5.7–9.3, mainly as consequence of the higher stiffening below the α peak temperature. It is also worth noting that the α peak of fibers with DR = 20 was detected in the range 34–37°C, i.e. at lower temperature than that of other drawn fibers (39–55°C).

Loss Modulus. The viscoelastic behavior of polyolefin fibers is mainly influenced by crystallinity, lamellar thickness, and amorphous layer thickness [31]. Similarly to storage modulus (E'), loss modulus (E'') of the HDPE/LDH composite fibers increased with the draw ratio and LDH content (Fig. 2a–d). In particular, nanocomposite fibers LDH-1 showed the highest values of loss modulus. The nanofiller effect on the stiffening of drawn fibers was found to decrease in following order

$$\text{LDH-1} \gg \text{LDH}-2,\ \text{LDH-1},\ \text{LDH-0.5} > \text{HDPE}$$

According to Stadler [16], α relaxation is related to the molecular motion in the crystalline phase as documented for PEs with different crystallinity contents.

For DR = 1, α relaxation peak is slightly higher for compositions with 2 and 3 wt% of nanofiller, 164 MPa with respect to 154 MPa for HDPE (Table 3). As already documented by other researchers, higher crystallinity of PE accounts for a higher α peak [13, 32]; in the same time, the α peak is shifted to lower temperature (Table 2), for example from 45 to 38°C for neat HDPE and for LDH-3, respectively. Following to Popli et al. [33], the lower the crystalline thickness, the lower the temperature of the α peak of PEs with almost the same degree of crystallinity 40%. However, also other parameters could be taken into account in order to interpret the α relaxation, such as crystallinity, crystalline perfection, microstructure of the crystalline phase [34], polymer chains

TABLE 3. Loss modulus peak of neat and nanofilled HDPE fibers as a function of the LDH volume fraction (Φ_f).

Fiber	Φ_f	E'' peak (MPa)	E''_C/E''_M	Φ_e	*B*
DR = 1					
HDPE	0	154	1.00	0	–
LDH-0.5	3.7×10^{-2}	155	1.00	0.006	1.62
LDH-1	7.4×10^{-2}	160	1.04	0.037	5.00
LDH-2	14.8×10^{-2}	164	1.06	0.061	4.12
LDH-3	22.2×10^{-2}	164	1.06	0.061	2.74
DR = 5					
HDPE	0	432	1.00	0	–
LDH-0.5	3.7×10^{-2}	585	1.35	0.262	70.8
LDH-1	7.4×10^{-2}	1175	2.72	0.632	85.4
LDH-2	14.8×10^{-2}	858	1.99	0.497	33.5
LDH-3	22.2×10^{-2}	682	1.58	0.367	16.5
DR = 10					
HDPE	0	1166	1.00	0	–
LDH-0.5	3.7×10^{-2}	2539	2.18	0.541	146.2
LDH-1	7.4×10^{-2}	3848	3.30	0.697	94.2
LDH-2	14.8×10^{-2}	2565	2.20	0.545	36.8
LDH-3	22.2×10^{-2}	2286	1.96	0.490	22.1
DR = 20					
HDPE	0	1676	1.00	0	–
LDH-0.5	3.7×10^{-2}	2400	1.43	0.302	81.6
LDH-1	7.4×10^{-2}	4300	2.56	0.610	82.4
LDH-2	14.8×10^{-2}	3004	1.79	0.442	29.9
LDH-3	22.2×10^{-2}	3121	1.86	0.463	20.8

Effective volume fraction of the dispersed phase,(φ_e) and *B* parameter were calculated according to the model proposed by Sumita et al. [37].

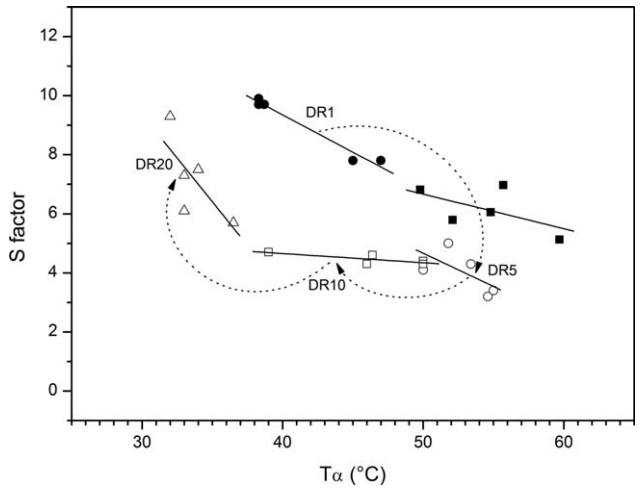

FIG. 4. Relationship between the S-factor and the α peak temperature, Tα, of as-spun fibers (●), and fibers with draw ratio 5 (○), 10 (□), and 20 (Δ). Plates data (■) refer to HDPE and HDPE nanocomposite with 0.5, 1, 2, and 5% of LDH (from Dabrowska et al. 5).

orientation in fibers and filaments, etc. [35, 36]. Perena et al. [35] reported that HDPE mofilament after drawing exhibited not only an increase in both storage and loss modulus, but also a significant decrease in the temperature of the α peak.

An interesting relationship between the temperature of the α peak (Tα) and the S-factor is depicted in Fig. 4. The values of as-spun fibers are reported in the upper zone of high S-factor and intermediate Tα, between 38 and 48°C. After drawing at DR = 5, the α peak was found to shift toward higher temperatures as an effect of increased crystallinity from 50–53% to about 65%, along with a parallel decrease in the *S*-factor. At higher draw ratios 10–20, the α peak was shifted to lower temperature in conformity to literature data [36, 37], but in the same time the *S*-factor was found to increase for DR = 20. A possible explanation is a combined effect of the reduction of crystalline thickness and the increase in stiffening during high drawing. In analogy, corresponding data of the HDPE/LDH plates [5] obtained by compression molding (crystallinity of 70–72%) are also shown in Fig. 4. The results of plates exhibit higher temperature of α peak and lower *S*-factor, due to the high crystalline and not oriented polymer, and appear to follow the trend found for the as-spun fibers.

The magnitude of the loss modulus peak (Table 3) increased proportionally to the draw ratio and/or nanofiller fraction; the highest intensities were obtained for the compositions with 1 and 2 wt% of LDH. These results can be elucidated by sufficient LDH layer intercalation and exfoliation in the HDPE matrix when the nanofiller content is optimal. Higher values of the storage and loss modulus observed for drawn material are related to the increase in the fraction of crystalline phase induced during drawing. Moreover, after drawing LDH exhibits a stronger interfacial interaction with the matrix, thereby limiting the molecular mobility [26].

The β relaxation could depend on various factors, such as crystallinity, amorphous phase orientation, and/or nanofiller addition. Figure 2a related to as-spun fibers of HDPE/LDH nanocomposites did not show any transition in the temperature interval between the γ and α relaxations. On the other hand, for DR = 5 and 10 a small β relaxation appeared as a shoulder between −80 and 0°C (Fig. 2b and c), in particular for the composition with 1 wt% of hydrotalcite. However, in Fig. 2d for DR = 20, the β transition is not visible, probably due to high orientation of polymer chains. Some authors related the β relaxation to the movement of the chain units in the interfacial region [13, 32], others to the relaxation of short chain branches or the amorphous phase [38]. The observed intensification of the β relaxation was tentatively attributed to restricted segmental motions at the PE/filler interface [39].

Sumita et al. [37] utilized the dissipation energy in dynamic mechanical measurements to specify the effective volume fraction of the dispersed phase, Φ_e, which is composed of the volume of filler plus that of the "immobilized matrix layer" adjacent to the interface. The parameter *B* is used to describe the relative value of the effective volume per a single particle, as shown in *Eq. 3*:

$$\frac{E''_C}{E''_M} = 1 - \Phi_e)^{-1} = (1 - \Phi_f B)^{-1} \quad (3)$$

where E''_C and E''_M represent the maximal loss moduli of the composites and of the neat polymer matrix at the respective loss peaks.

To characterize the interphase thickness, the effective particle volume fraction (Φ_e) and effective volume per single particle (B-parameter) were calculated, as reported in Table 3 and in Fig. 5. For DR = 1 the effective particle volume fraction does not change with volume fraction of the filler, while for drawn fiber Φ_e increases with the filler content up to about 0.7 vol%, whereas further addition of LDH brings about a dramatic decrease (Fig. 5a). Similar behavior was observed in the case of the B parameter (Fig. 5b). According to Sumita [32], Φ_e independent of increasing amount of the filler indicates that the thickness of the physically absorbed matrix layer on the surface of the nanofiller is limited, due to the agglomeration of the nanoparticles. In addition, decreasing B-parameters suggest that the extent of the particle agglomeration was increased with the filler content.

Creep

Creep analysis and modeling is fundamental for application perspectives, especially when polymer must sustain loads for very long times [25]. There have been several attempts to enhance the creep resistance of HDPE via crosslinking, copolymerization, and the use of additives and fillers. Figure 6 show the effect of increasing draw ratio on the isothermal creep compliance curves at 30°C

 DOI 10.1002/pc

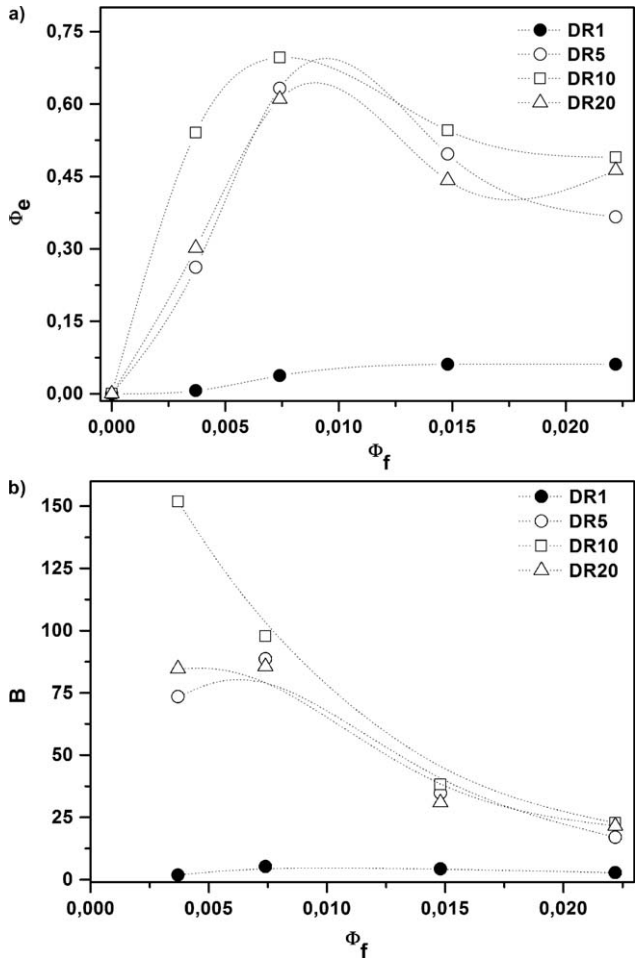

FIG. 5. (a) Effective particulate volume fraction, (Φ_e), and (b) effective particulate volume per single particle (B), of HDPE-LDH nanocomposites as a function of LDH volume fraction. Draw ratios: DR = 1 (●); DR = 5 (○); DR = 10 (□); black symbol—DR = 20 (Δ).

for neat HDPE and nanocomposite fibers (constant load of 3 MPa for 3600 s). For as-spun fibers, the creep compliance for the compositions with a low amount of nanofiller (0.5–1 wt%) was practically equal to that of the neat HDPE, while for compositions with 2 and 3 wt% of LDH the creep compliance was slightly enhanced. For drawn material it is evident that the incorporation of hydrotalcite leads to a reduction of the creep compliance. Creep resistance of the composites with nanofiller amount (0.5 and 1 wt%) was again found higher than that of fibers with 2 and 3 wt% of LDH. It has also been proven by other authors [40–42] that an introduction of layered silicates reduces the creep compliance; moreover, the level of intercalation and/or exfoliation codetermines the final creep resistance of nanocomposites [11, 12, 43].

As the drawing process caused a better dispersion and orientation of the nanofiller in the HDPE/LDH nanocomposites, a lower creep compliance than that of the neat HDPE fibers was found (Fig. 6b). For 0.5 and 1 wt% of LDH, TEM analysis evidenced a good dispersion after drawing process, whereas for higher nanofiller fractions some aggregates were present. These different creep dependencies could be attributed to the nanofiller dispersion and/or aggregation, in dependence on its concentration. As for higher drawing ratios (up to DR = 20), the reduction of creep compliance is less significant (see Fig. 6c), we can conclude that the maximum physical interaction matrix/filler was achieved at lower DRs, while further increase in DR did not bring any perceptible improvement.

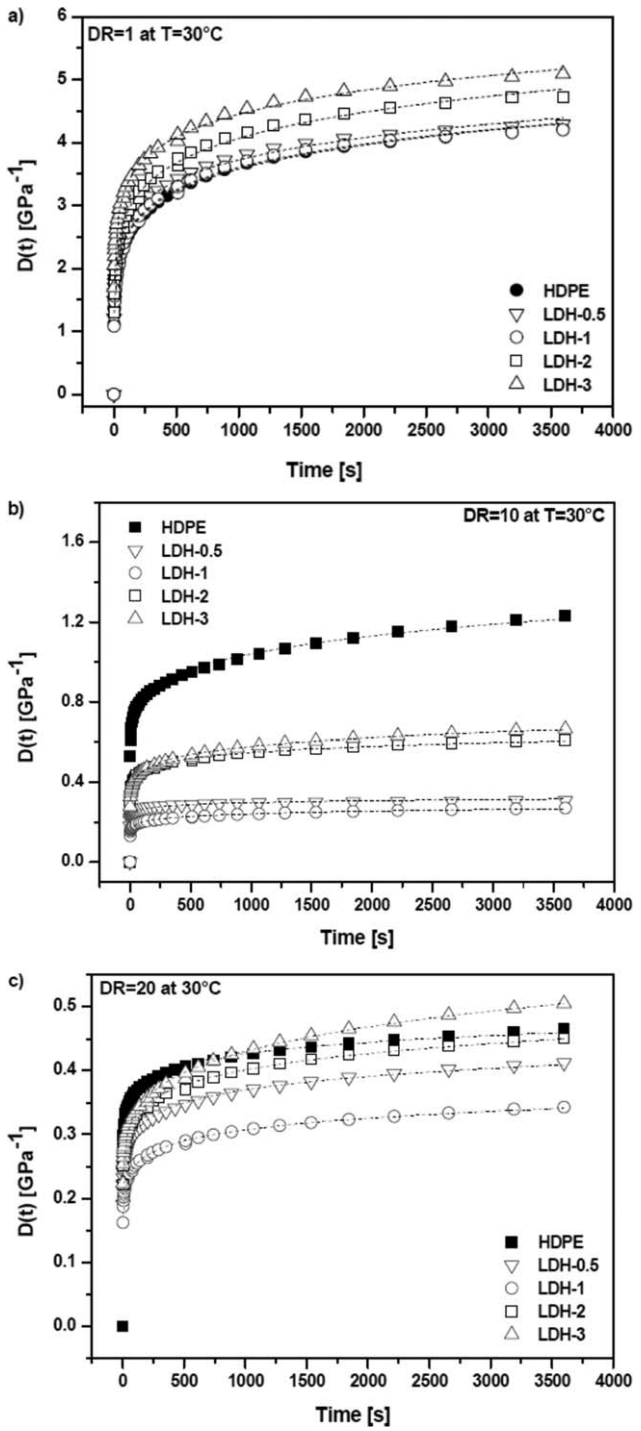

FIG. 6. Tensile compliance of neat and nanofilled HDPE fibers as a function of time. Stress $\sigma_0 = 3$ MPa; temperature 30°C; draw ratio: (a) DR = 1, (b) DR = 10, and (c) DR = 20.

TABLE 4. Elastic (E_M and E_K) and viscous (η_M and η_K) parameters of the Burgers model characterizing the creep compliance of polyethylene/hydrotalcite nanocomposite fibers in isothermal creep tests at $T = 30°C$ ($\sigma_0 = 3$ MPa).

Fiber	E_M (MPa)	η_M (GPa s^{-1})	E_K (MPa)	η_K (GPa s^{-1})	R^2
DR = 1 at 30°C					
HDPE	0.86 ± 0.13	2.4 ± 0.6	0.54 ± 0.07	0.36 ± 0.03	0.928
LDH-0.5	0.82 ± 0.22	2.5 ± 0.6	0.52 ± 0.06	0.29 ± 0.06	0.920
LDH-1	0.88 ± 0.27	2.5 ± 0.6	0.52 ± 0.07	0.35 ± 0.06	0.930
LDH-2	0.58 ± 0.08	2.8 ± 0.4	0.55 ± 0.10	0.65 ± 0.05	0.978
LDH-3	0.46 ± 0.16	2.8 ± 0.4	0.55 ± 0.10	0.60 ± 0.11	0.973
DR = 10 at 30°C					
HDPE	1.6 ± 0.4	6.7 ± 1.2	1.4 ± 0.2	4.70 ± 0.7	0.910
LDH-0.5	16.6 ± 0.1	50.0 ± 5.8	8.4 ± 0.2	3.82 ± 0.8	0.930
LDH-1	14.1 ± 0.2	33.3 ± 7.6	18.2 ± 2.0	4.50 ± 0.6	0.920
LDH-2	2.9 ± 1.1	33.3 ± 3.9	6.7 ± 1.5	5.05 ± 1.0	0.961
LDH-3	3.0 ± 0.5	20.0 ± 4.8	5.7 ± 1.0	4.97 ± 1.5	0.966
DR = 20 at 30°C					
HDPE	3.9 ± 1.4	16.4 ± 1.2	7.0 ± 1.2	7.0 ± 1.5	0.930
LDH-0.5	4.4 ± 0.9	38.4 ± 2.6	72.2 ± 11.2	6.2 ± 1.8	0.960
LDH-1	5.3 ± 1.1	50.0 ± 2.3	78.3 ± 10.0	9.3 ± 2.3	0.970
LDH-2	3.9 ± 0.8	37.0 ± 2.9	67.1 ± 11.5	8.4 ± 0.5	0.970
LDH-3	3.8 ± 0.7	26.3 ± 3.4	57.8 ± 9.1	10.0 ± 1.5	0.973

Several models have been developed to represent the response of a viscoelastic material under creep conditions. We have found the Burgers model useful to separate and interpret the elastic and viscoelastic components of measured compliance. The Burgers model [44] combines the Maxwell and Kelvin models coupled in series:

$$D(t) = \frac{1}{E_M} + \frac{t}{\eta_M} + \frac{1}{E_K}\left(1 - e^{\frac{E_K t}{\eta_K}}\right) \quad (4)$$

where E_M, η_M are elastic and viscous components of the Maxwell model, and E_K, η_K are elastic and viscous components of the Kelvin model [25].

Dot lines in Fig. 6 represent the best fitting of the experimental creep compliance curves by the Burgers model; the corresponding parameters are reported in Table 4. As can be seen, higher elastic (E_K, E_M) and viscous components (η_K η_M) were found for drawn fibers. Comparing the fitting parameters of the neat HDPE and nanofilled drawn fibers, we can conclude that the parameters reflecting the elastic or viscous response of nanocomposites are higher than those found for the matrix. Specifically, much higher η_M were observed for drawn LDH-0.5 and LDH-1 fibers, either at DR = 10 or DR = 20. Similar behavior reported [45] for polyamide fibers was explained in such a way that η_M controls the creep for long times, which evidences reinforcing effect of well-dispersed hydrotalcite in drawn fibers.

The temperature dependence of the tensile creep response of the HDPE-based nanocomposite fibers was also studied at temperatures above the α transition. Figure 7 shows a much higher creep compliances at 70°C of both HDPE and LDH nanocomposites fibers (stress of 3 MPa for 3,600 s) in comparison with Fig. 6. It can be

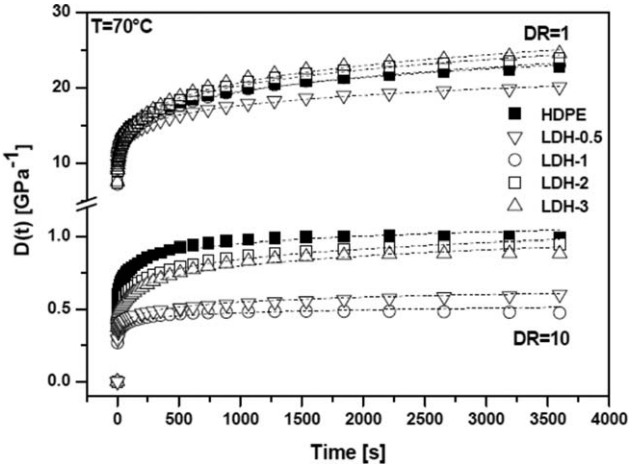

FIG. 7. Tensile compliance of neat and nanofilled HDPE fibers as a function of time. Stress $\sigma_0 = 3$ MPa; temperature 70°C; draw ratio DR = 1 and DR = 10.

seen that the compliance of as-spun fibers (DR = 1) is virtually independent of the nanofiller fractions. In contrast at DR = 10, the presence of hydrotalcite is manifested by a distinctly lower creep compliance, especially in the interval of filler fractions 0.5–1 wt%, which is analogous to the results observed for 30°C. As expected, all the elastic (E_M, E_K) and viscous (η_M, η_K,) parameters of the Burgers model decline with temperature (Table 5). Obviously, better creep resistance of drawn fibers at 70°C can be attributed to higher η_M and E_K components of the Maxwell and Kelvin models, respectively. Similarly enough, lower creep compliance at 70°C of LDH-05 and LDH-1 fiber (DR = 10) can be related to higher elastic component E_M, as also observed at 30°C.

We can conclude that creep resistance of HDPE has significantly been enhanced by the incorporation of hydrotalcite nanoparticles. Our results evidence that small and well-dispersed amounts of the filler have plausible reinforcing effects, especially in drawn fibers. However, it should be pointed out that the effect is not linearly

TABLE 5. Elastic (E_M and E_K) and viscous (η_M and η_K) parameters of the Burgers model characterizing the creep compliance of polyethylene/hydrotalcite nanocomposite fibers in isothermal creep tests at $T = 70°C$ ($\sigma_0 = 3$ MPa).

Fiber	E_M (MPa)	η_M (GPa s^{-1})	E_K (MPa)	η_K (GPa s^{-1})	R^2
DR = 1 at 70°C					
HDPE	0.68 ± 0.02	0.33 ± 0.03	0.07 ± 0.01	0.33 ± 0.06	0.875
LDH-0.5	0.73 ± 0.03	0.42 ± 0.04	0.08 ± 0.02	0.34 ± 0.06	0.888
LDH-1	0.64 ± 0.02	0.39 ± 0.03	0.11 ± 0.07	0.38 ± 0.05	0.898
LDH-2	0.60 ± 0.03	0.39 ± 0.02	0.10 ± 0.05	0.51 ± 0.02	0.899
LDH-3	0.58 ± 0.04	0.40 ± 0.02	0.10 ± 0.06	0.67 ± 0.07	0.887
DR = 10 at 70°C					
HDPE	1.28 ± 0.23	10.6 ± 2.4	1.45 ± 0.8	6.3 ± 0.1	0.825
LDH-0.5	1.03 ± 0.18	9.7 ± 5.1	10.8 ± 0.2	1.8 ± 5.2	0.820
LDH-1	10.2 ± 2.1	12.2 ± 4.1	34.5 ± 3.8	18.3 ± 3.5	0.830
LDH-2	1.05 ± 0.09	11.1 ± 2.3	18.4 ± 4.5	9.61 ± 3.2	0.840
LDH-3	1.39 ± 0.21	16.9 ± 4.2	28.5 ± 2.4	12.2 ± 5.1	0.840

DOI 10.1002/pc

proportional to the filler content: the optimal filler concentrations range between 0.5 and 1 wt%, whereas at higher concentration, hydrotalcite tends to form aggregates which have a detrimental effect on mechanical properties of the fibers.

CONCLUSIONS

Viscoelastic properties of the HDPE/hydrotalcite nanocomposite fibers show a remarkable dependence on the composition and/or the drawing process. In particular, DMTA tests evidence the stiffening effect of the hydrotalcite nanofiller incorporated in HDPE matrix, which is manifested by higher storage moduli for all composite fibers, especially at higher draw ratios. A relative maximum of the storage modulus occurs at 1% of LDH.

The position of the α transition peak is significantly affected by the drawing; its temperature increases at low draw ratios, and then shifts to lower temperature at high draw ratios. Moreover, the intensity of this transition (S-factor) indicates significant differences between as-spun and drawn fibers, which depend on their crystallinity, orientation and stiffening, but are almost independent of the LDH content.

TEM analysis of the composites with 0.5 wt% filler shows a very good dispersion of hydrotalcite in HDPE, both in as-spun and drawn fibers, and a progressive reduction of aggregates with the draw ratio. The effective particle volume fraction and the effective volume per single particle (according to the Sumita model) exhibits maximum values for compositions with 0.5 and 1% of LDH, especially for drawn fibers.

Creep tests evidence the reinforcing effect of LDH manifested by a noticeable reduction of the creep compliance (with respect to that of the neat HDPE fibers) over the whole ranges of investigated draw ratios and temperatures. Improvements in mechanical properties of the nanofilled fibers require (i) the specimens with uniform dispersion of hydrotalcite particles, which makes possible to achieve (ii) high draw ratios promoting both crystallization and molecular orientation. Thus, it can be concluded that LDH nanoparticles effectively reinforce HDPE fibers, particularly at higher draw ratio. The best balanced mechanical properties were found for the nanocomposite of HDPE with 1 wt% of LDH.

ACKNOWLEDGMENTS

The authors thank Dr. Marco Casinelli and Dr. Roberta Selleri (LyondellBasell Industries—Basell Poliolefine Italia S.r.l. "Giulio Natta" R&D) for TEM analysis, and Clariant Masterbatches S.p.A. (Italy) for donating the HDPE perkalite masterbatch used in this study. The authors are greatly indebted to Professor Jan Kolarik (Institute of Macromolecular Chemistry, Prague) for his valuable comments.

NOMENCLATURE

B	parameter of Sumita model
D	tensile compliance
DMTA	dynamical mechanical thermal analysis
DR	draw ratio
E_K	elastic component of the Kelvin model
E_M	elastic component of the Maxwell model
E'	storage modulus
E'_{-30}	storage modulus at −30°C
E'_{90}	storage modulus at 90°C
E''	loss modulus
E''_C	loss modulus of composite
E''_M	loss modulus of matrix
HDPE	high density polyethylene
HDPE/LDH	High density polyethylene/layered double hydroxide
η_K	viscous component of the Kelvin model
η_M	viscous component of the Maxwell model
LDH	layered double hydroxide
LDPE	low density polyethylene
LLDPE	linear low density polyethylene
MA	maleic anhydride
PE	polyethylene
PP	polypropylene
σ_0	stress of creep test
S	intensity of transition
SEM	scanning electron microscopy
Tα	temperature of a-peak
TEM	Transmission electron microscopy
UHMWPE	Ultra high molecular weight polyethylene
Φ_e	effective volume fraction of the dispersed phase
Φ_f	volume fraction of the filler
XRD	X-ray diffraction

REFERENCES

1. A.J. Peacock, *Handbook of Polyethylene: Structures, Properties and Applications*, (pp. 27–42) Marcel Dekker, New York (2000).
2. R.R. Mather, "The Structure of Polyolefin Fibres," in *Handbook of Textile Fibre Structure: Fundamentals and Manufactured Polymer Fibres*, S. Eichhor, J.W.S. Hearle, M. Jaffe, and T. Kikutani Eds., (Ch. 9, pp. 276–304) Woodhead Publishing in Textiles, Boca Raton FL, (2009).
3. I.M. Ward and P.J. Lemstra, "Production and Properties of High-modulus and High-strength Polyethylene Fibers," in *Handbook of Textile Fibre Structure: Fundamentals and Manufactured Polymer Fibres*, S. Eichhor, J.W.S. Hearle, M. Jaffe, and T. Kikutani Eds., (Ch. 12, pp. 352–393) Woodhead Publishing in Textiles, Boca Raton FL, (2009).
4. C. Marega, V. Causin, A. Marigo, G. Ferrara, and H. Tonnaer, *J. Nanosci. Nanotechnol.*, **9**, 2704 (2009).
5. I. Dabrowska, L. Fambri, A. Pegoretti, and G. Ferrara, *Express Polym. Lett.*, **7**, 936 (2013).
6. L. Fambri, I. Dabrowska, A. Pegoretti, and R. Ceccato, *J. Appl. Polym. Sci.*, **131**, 40277 (2014).

7. F.R. Costa, A. Leuteritz, J. Meinl, U. Wagenknecht, and G. Heinrich, *Macromol. Symp.*, **301**, 46 (2011).
8. M. Ardanuy, J.I. Velasco, M. Antunes, M.A. Rodriguez-Perez, and J.A. de Saja, *Polym. Compos.*, **31**, 870 (2010).
9. J.L. White and D.D. Choi, *Polyolefins: Processing, Structure Development and Properties*, Hanser, Munich (2005).
10. F.P. La Mantia, N.T. Dintcheva, R. Scaffaro, and R. Marino, *Macromol. Mater. Eng.*, **293**, 83 (2008).
11. Y. Zhang, J. Yu, C. Zhou, L. Chen, and Z. Hu, *Polym. Compos.*, **31**, 684 (2010).
12. Z. Guo and B. Hagström, *Polym. Eng. Sci.*, **53**, 2035 (2013).
13. N.G. McCrum, B.E. Ready, and G. Williams, *Anelastic and Dielectric Effects in Polymeric Solids*, Wiley, New York (1967).
14. R.H. Boyd, *Macromolecules*, **17**, 903 (1984).
15. Y.P. Khanna, A. Turi, T.J. Taylor, V.V. Vickroy, and R.F. Abbott, *Macromolecules*, **18**, 1302 (1985).
16. F.J. Stadler, *Korean J. Chem. Eng.*, **28**, 954 (2011).
17. P. Starck and B. Löfgren, *Eur. Polym. J.*, **38**, 97 (2002).
18. J.J. Dechter, D.E. Axelson, A. Dekmezian, M. Glotin, and L. Mandelkern, *J. Polym. Sci. Polym. Phys.*, **20**, 641 (1982).
19. R.G. Matthews, A.P. Unwin, I.M. Ward, and G. Capaccio, *J. Macromol. Sci. B*, **38**, 123 (1999).
20. U. Costantino, A. Gallipoli, M. Nocchetti, G. Camino, F. Bellucci, and A. Frache, *Polym. Degrad. Stabil.*, **90**, 586 (2005).
21. F.R. Costa, M. Abdel-Goad, U. Wagenknecht, and G. Heinrich, *Polymer*, **46**, 4447 (2005).
22. F.R Costa, B.K. Satapathy, U. Wagenknecht, R. Weidisch, and G. Heinrich, *Eur. Polym. J.*, **42**, 2140 (2006).
23. B. Tuklu, J. Meinl, A. Leuritz, H. Brüning, and G. Heinrich, *Polymer*, **54**, 5712 (2013).
24. M. D'Amato, A. Dorigato, L. Fambri, and A. Pegoretti, *Express Polym. Lett.*, **6**, 954 (2012).
25. L.E. Nielsen, *Mechnical Properties of Polymers and Composite*, Marcel Dekker, New York (1974).
26. Y. Tian, H. Zhang, J. Qin, J. Yu, L. Cheng, and Q. Lv, *J. Compos. Mater.*, **48**, 245 (2014).
27. S.P. Lonkar, S. Therias, F. Leroux, J.-L. Gardette, and R.P. Singh, *Polym. Eng. Sci.*, **52**, 2006 (2012).
28. E. Kontou and M. Niaounakis, *Polymer*, **47**, 1267 (2006).
29. S. Díez-Gutiérrez, M.A. Rodríguez-Pérez, J.A. De Saja, and J.I. Velasco, *Polymer*, **40**, 5345 (1999).
30. L. Fambri, K. Kesenci, and C. Migliaresi, *Polym. Compos.*, **24**, 100 (2003).
31. G. Capaccio and I.M. Ward, *J. Polym. Sci. Polym. Phys.*, **22**, 475 (1984).
32. E. Passaglia, S. Coiai, G. Giordani, E. Taburoni, L. Fambri, V. Pagoni, and M. Penco, *Macromol. Mater. Eng.*, **289**, 809 (2004).
33. R. Poplin, M. Glotin, and L. Mandelkern, *J. Polym. Sci. Polym. Phys.*, **22**, 407 (1984).
34. R.H. Boyd, *Polymer*, **26**, 323 (1985).
35. J.M. Perena and J.M.G. Fatou, *An. Fis. (Madrid)* **70**, 348 (1974).
36. S.-D. Rong, H.L. Williams, *J. Appl. Polym. Sci.*, **30**, 2575 (1985).
37. M. Sumita, H. Tsukihi, K. Miyasaka, and K. Ishikawa, *J. Appl. Polym. Sci.*, **29**, 1523 (1984).
38. D.E. Kline, J.A. Sauer, and A.E. Woodward, *J. Polym. Sci.*, **22**, 455 (1956).
39. M. Alexandre and P. Dubois, *Mater. Sci. Eng.*, **28**, 1 (2000).
40. M. Joshi and V. Viswanathan, *J. Appl. Polym. Sci.*, **102**, 2164 (2006).
41. A. Pegoretti, J. Kolarik, C. Peroni, and C. Migliaresi, *Polymer*, **45**, 2751 (2004).
42. A. Ranade, K. Nayak, D. Fairbrother, and N.A. D'Souza, *Polymer*, **46**, 7323 (2005).
43. A. Pegoretti, "Creep and Fatigue Behavior of Polymer Nanocomposites," in *Nano- and Micro-mechanics of Polymer Blends and Composites*, J. Karger-Kocsis and S. Fakirov, Eds., (Ch. 9, pp. 301–339), Hanser Publications, Cincinnati (2009).
44. I.M. Ward, *Mechanical Properties of Solid Polymers*, Wiley, Weinheim (1983).
45. A. Dorigato and L. Fambri, *Polym. Compos.*, **32**, 786 (2011).

 DOI 10.1002/pc